2011 IEEE International Conference on Robotics and Automation
Shanghai International Conference Center
May 9-13, 2011, Shanghai, China

Real-time feedback control using artificial magnetotaxis with rapidly-exploring random tree (RRT) for *Tetrahymena pyriformis* as a microbiorobot

Dal Hyung Kim*, Sean Brigandi*, Anak Agung Julius† and Min Jun Kim*

Abstract— **In this paper, we present a control strategy using real-time feedback combined with feasible path planning to manipulate a type of microorganism, *Tetrahymena pyriformis* (*T. pyriformis*), as a micro-bio-robot using artificial magnetotaxis. Artificially magnetotactic *T. pyriformis* cells were created by the internalization of iron oxide nano particles. Following the magnetization of the internalized particles, the cells become controllable using an external time-varying magnetic field. The behavior of artificially magnetotactic *T. pyriformis* under a magnetic field has been investigated in a manual control experiment. A feasible path planner called rapidly-exploring random tree (RRT) and a feedback control scheme are implemented to guide the cell to a desired position and orientation. Since the motion of *T. pyriformis* is nonlinear like that of a car, combining the RRT and feedback control allows the cell to be controlled in 3-dimensional (x, y, θ) space. In the results, real-time feedback control of *T. pyriformis* in 3-dimensional space demonstrated the potential of utilizing *T. pyriformis* as a micro-bio-robot for microscale tasks.**

Keywords: *Tetrahymnea pyriformis*, Artificial magnetotaxis, Real-time feedback control, Rapidly-exploring random tree (RRT), Microbiorobot

I. INTRODUCTION

Microrobots in low Reynolds number fluidic environments have been investigated for micro-scale applications such as transportation, delivery, and assembly using artificial robots or biological robots. For artificial microrobots, fabrication of miniature actuator for microfludic environments is the key. Some researchers have investigated artificial microrobots by mimicking motile organelles such as flagella [1]–[3] using microelectromechanical systems (MEMS) technology. Other researchers have utilized magnetic forces and stick slip motions to reduce friction forces to manipulate microrobots [4, 5] . Even though artificial microrobots have an advantage of robust control, supplying sufficient power sources for the microrobots in a microfludic environment is a key challenge.

Another approach in microrobotics is to utilize live microorganisms as actuators. Microorganisms have cellular motors, such as flagella and cilia, which exert mechanical swimming forces by drawing chemical energy from their fluidic environments. Magnetic bacteria [6]–[8], which have nanometer-sized magnetosomes inside of the cell have been studied to control their motion using magnetic fields. Bacterial propulsion forces have been exploited to manipulate microbeads [9]. Controlling and sensing of bacteria blotted on the microstructures have been studied as well [10, 11]. Furthermore, the movements of eukaryotic cells such as T*etrahymena pyriformis* (*T. pyriformis*) [12], *Euglena* [13], and *Paramecium* [14, 15] have also been studied and demonstrated. Microorganisms as a microrobot can be used as a sensor using many taxes such as chemotaxis, galvanotaxis and phototaxis. However, despite these advantages, only some tactic movement and simple control have been demonstrated. This can be attributed to the difficulty of controlling microorganisms due to their low response rate, as well as implementing them with the controllable system.

In this paper, we have utilized an artificial magnetotactic organism with *T. pyriformis* using iron oxide particles, and developed a system to accomplish real-time feedback control. Unlike magnetic bacteria [6]–[8], the artificial magnetotactic *T. pyriformis*, when it is controlled moves using its endogenous motility, not a magnetic force. The magnetic field exerts only a torque, which allows for the change of the cell's swimming direction, while the cell's velocity is not controllable. Due to the nonlinear motion of the cell, a feasible path planning method called rapid-exploring random tree (RRT) is implemented which allows us to control the cell to a desired position by controlling the swimming direction. Since the artificial taxis and endogenous motility of the cell are integrated into one system, the magnetotactic organism can be controlled robustly while the actuation force is exerted from the cell. We have shown that manual control can be used to understand the motion of artificially magnetotactic *T. pyriformis*, and that combining real-time control with the feasible path planning scheme have verified the possibility of using *T. pyriformis* as a micro-bio-robot.

II. MATERIALS AND METHODS

A. Cell culture

T. pyriformis is a eukaryote which is a 50 μm long and 20 μm wide pear-shaped cell. The entire body of the cell is covered with about 600 cilia which makes the cell motile. *T. pyriformis* is cultured in the culture medium which includes 0.1% yeast extract (Difco, Michigan, USA) and 1% Bacto tryptone (Difco, Michigan, USA) in distilled water [16]. The saturated culture has 10^4 cells·ml^{-1} of the cell density. The cell culture medium was diluted with a fresh culture medium in a 1:3 ratio (working cell density was $3.3 \cdot 10^3$ cells·ml^{-1}) in

*Department of Mechanical Engineering and Mechanics, Drexel University, Philadelphia, PA 19104, USA Dalhyung.Kim, Sean.E.Brigandi@drexel.edu, mkim@coe.drexel.edu,
†Department of Electrical, Computer and Systems Engineering, Rensselaer Polytechnic Institute, Troy, NY 12180, USA agung@ecse.rpi.edu

order to lower the cell concentration for single cell detection and tracking over a long period of time.

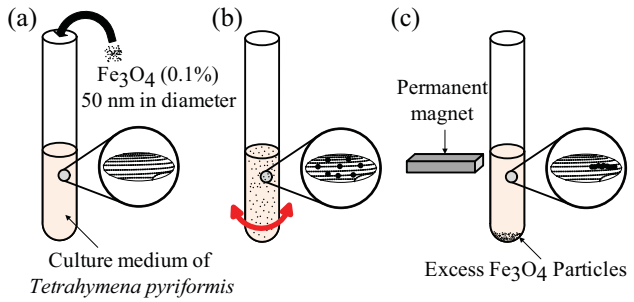

Fig. 1. The procedure for fabrication of artificially magnetotactic *T. pyriformis* from (a) to (c). (a) Addition of iron oxide particles (magnetite, Fe_3O_4) particles into the culture medium. (b) Gentle agitation to ensure the cells internalize the iron oxide particles. (c) Magnetization of the internalized magnetite using a permanent magnet.

B. Fabrication of artificially magnetotactic T. pyriformis

Figure 1 shows the process to create the artificially magnetotactic *T. pyriformis* [17]. In Figure 1 (a), 0.1% iron-oxide spherical particles (Sigma Aldrich, MO, USA) whose size is about 50 *nm* in diameter are added into the culture medium. When iron oxide particles (magnetite) are added, *T. pyriformis* internalize the magnetite via an oral apparatus located at the anterior part of cell. The internalized magnetites are stored in membrane bounded vesicles which are shown as dark circles in Figure 1 (b). The magnetite loaded *T. pyriformis* is physiologically intact and its swimming behavior is identical to the normal cell [18]. Even though internalization of iron oxide particles takes place right after the particles are supplemented, the culture medium with iron-oxide particles is gently agitated and left for 10 minutes to ensure sufficient internalization of the magnetite. Figure 1 (c) shows the magnetization process of the internalized ferromagnetic magnetite. A rectangular neodymium-iron-boron (NdFeB) permanent magnet with a surface field of 1964 Gauss (K&J Magnetics, PA, USA) is applied around the cell culture for about one minute to magnetize the internalized magnetite, and sequentially cause the magnetite to aggregate. A permanent magnet emits a strong magnetic field to ensure magnetization of the magnetite. After the permanent magnet is removed after magnetization, the strength magnetic dipoles remain nearly constant for over one hour; therefore, it is assumed that the internalized magnetite is saturated during the experiments. However, the magnetic dipoles will diminish over a period of time because the magnetic state of the ferromagnetic material is a hysteresis function of the strength of the applied magnetic field [19].

III. Feedback Control and Path Planning

A. Experimental Setup

Figure 2 (a) shows the system for feedback control of the magnetotactic *T. pyriformis*, which includes a microscope, a camera, a computer, a control board, two power supplies,

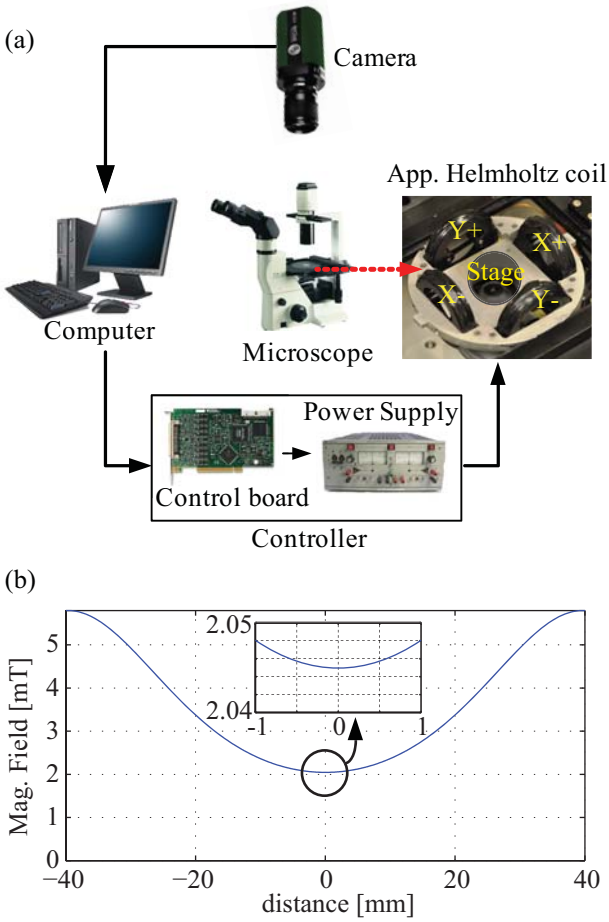

Fig. 2. The magnetic control and vision system for real-time control of artificially magnetotactic *T. pyriformis*: (a) system drawing and (b) the strength of the magnetic field in the center. Nearly constant magnetic field is created in the field of view.

and a set of approximate Helmholtz coils. The microscope and camera are used for capturing the images of the cell motion and the computer is used for cell tracking. Based on the tracked data, the feedback inputs are sent through the control board to the power supplies which provide power to the approximate Helmholtz coils to generate magnetic fields in a two-dimensional system. Figure 2 (b) illustrates the exerted magnetic fields by the approximate Helmholtz coils. Since the coils for *x*- and *y*-axes are identical, only a one-dimensional magnetic field is illustrated. The field of view through the microscope is limited in 2 *mm* for each axis. In this field of view, the magnetic field is about 2 *mT* and approximately constant, which is described in the small window in Figure 2 (b).

B. Cell detecting (tracking) and Modeling

To detect and track the positions of *T. pyriformis*, a real time tracking algorithm was implemented. A camera connected to the microscope captured sequence of images which were imported and digitized by the image processing program to detect positions of the cell [12]. Figure 3 shows a cell model for *T. pyriformis*. The configuration of a cell

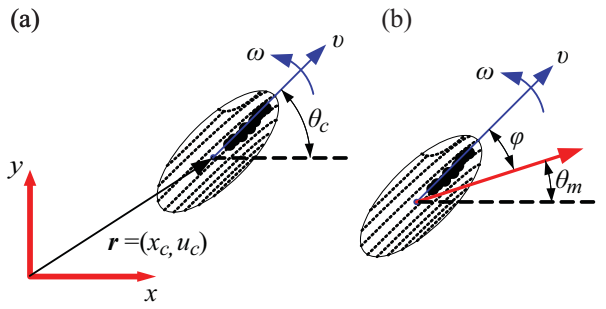

Fig. 3. A schematic of the artificially magnetotactic *T. pyriformis*. The configuration includes the centroid (x_c, y_c) and orientation (θ_c) of the cell. The translational velocity and angular velocity are represented by υ and ω respectively. The angle (θ_m) is the direction of the magnetic fields and ϕ is the angle between the θ_c and θ_m.

is represented by x_c, y_c, and θ_c; which are x, y position, and an angle of orientation of the major axis from x-axis. Translation and rotation velocities are represented by υ and ω, respectively.

C. Magnetized cell behavior under the magnetic field

When magnetites are magnetized, magnetite aggregations are normally observed along the major axis of the cell body. The polarity of the internalized magnetite aggregation depends on the swimming direction when the permanent magnet is applied for the magnetization. Thus, each individual cell has a polar magnetotaxis but some cells can have the opposite polarity. After magnetization, the cell freely swims without magnetic fields. However, when the magnetic fields are applied, the internalized magnetite exerts a torque on the cell to align the polarity with the magnetic fields. As a result, the cell moves toward the magnetic pole.

The angle between θ_m and θ_c which is represented by ϕ described in Figure 3 creates the torque on the cell by the following equation.

$$T = mB\sin(\theta_m - \theta_c) = mB\sin(\varphi) \tag{1}$$

where m is the magnetic momentum, B is the strength of the magnetic field.

D. Path planning by Rapidly-Exploring Random Tree

The dynamics of a *T. pyrifomis* cells motion is nonlinear and similar to that of a car. When it is being controlled, a *T. pyrifomis* swims forward only and changes direction with a turning radius. To fully manage the motion of this cell, both translational and rotational velocities should be controllable. However, since we are only able to manipulate the rotational velocity using the magnetic fields, magnetotaxis of *T. pyrifomis* is not sufficient for complete control of the cell motion. In the case of *T. pyriformis*, the translation velocity is controlled by the cell itself while only the angular velocity can be manipulated by the magnetic field.

Controlling the motion of *T. pyriformis* is a problem similar to one found for a car parking-assistant system which only controls the steering angle. For a parking assistant system, the translational velocity is controlled by the driver for safety reasons [20]. To accomplish autonomous car parking-assistance without controlling the translational velocity, feasible path planning is an essential scheme. Like a parking-assistant system, the feasible path planning scheme is required with feedback control to guide the cell to the desired configuration (x, y, θ).

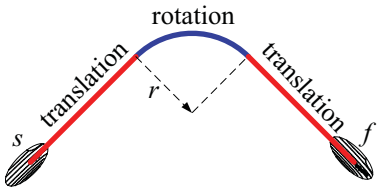

Fig. 4. The basic motions for the local path planner of RRT. Translation-rotation-translation is one set of basic motions.

1) Local path planner: For path planning, the basic motions are defined as translational and rotational motion. The translational motion is forward swimming movement without turning and the rotation motion is radial swimming movement with a turning radius. A local path is defined as translation-rotation-translation motion in sequence, which is described in Figure 4. Two arbitrary configurations can be connected many different ways [21]. However, the combinations are limited because a cell can only move forward; in some cases, there are no local paths which connects two configurations. After finding a local path, the existence of the path in the field of view is checked. Since there is no obstacle in our experiments, collision avoidance is not considered in this experiment.

2) Global path planner: To find the global path between two configurations rapidly-exploring random tree (RRT) [22, 23], one of the fastest path planning schemes, is used. First, we set the turning radius of the cell. We then randomly generate N points in the state space of the system (x, y, θ). We can then define a directed graph structure called a roadmap, in which the N points are the vertices. Any two vertices p_1 and p_2 in the graph are connected by an edge using the local path planner. Note that this calculation is performed offline. During the motion, our RRT path planning algorithm finds a path in the graph connecting the initial and goal positions.

Even though the start and final nodes are added on the roadmap, it is possible to fail to find a path through the roadmap due to the absence of connections between the two nodes. In this case, the RRT repeats the planning process on the next time step because the system is controlled in real-time. Also since the translational velocity is not controllable, only the start configuration of the cell is changed. Thus, instead of putting in a great deal of effort to connect the start and goal nodes, another path can be found on the next step with the new start configuration. Once the feasible path is found, a sequence of intermediate targets is generated on the feasible path as a trajectory.

E. Point to point Feedback control

Feedback control of the cell swimming direction is achieved by changing the direction of the magnetic field in order to guide a cell to reach a single target point from its current position. The strength of the magnetic field in the center is constant but the direction (θ_m) is adjusted by manipulating two sets of Helmholtz coils in the x and y axes. Once the cell reaches the intermediate target, the cell continues to follow the next target until the cell arrives at the final configuration.

IV. Results and Discussion

A. Manual control

To observe and characterize the motion of *T. pyriformis* under the magnetic field, an experiment was conducted using manual control in a polydimethylsiloxane (PDMS) channel. The magnetic fields were controlled with a keyboard by changing the positive and negative directions on either the *x*- or the *y*-axis. The PDMS channel was fabricated with a depth of 80 μm to give cells sufficient freedom to swim while keeping them in focus for visualization. A single *T. pyriformis* cell was controlled for 90 seconds. Figure 5 illustrates the data only from first 15 seconds due to the readability of figures. The images were captured and processed at 8 frames per second. Figure 5 (a) shows the trajectories of the cell while it was controlled to stay inside of the field of view. Figure 5 (b) shows the direction of magnetic fields (red dot line) and the cell motion (blue dot line) which is identical to the cell orientation. In Figure 5 (b) we can observe the transient response of the cell orientation with respect to the change in the magnetic field's direction.

From the experiment in Figure 5, the relationship between the angular velocity ω and the angle ϕ, which is the difference between angles of the cell orientation and the magnetic fields, is shown in Figure 6. The data from the manual control experiment was collected for 90 seconds for reliability. In Figure 6, it can be seen that angular velocity ω and $\sin(\phi)$ have a linear relationship which means that the angular velocity also has a linear relation with the torque T from equation (1).

When the direction of the magnetic field changes, *T. pyriformis* needs time to respond as explained previously. Since this experiment changes the direction of the magnetic field to the right angle from the direction of the cell motion ($\phi = 90°$), there are many points around $\sin(\phi) = \pm 1$ which do not have a linear relationship with the angular velocity because these points represent the transient response of the cell. Thus, these data points should be excluded when computing the linear relationship. The next step in our research is to utilize system identification techniques in formally deriving a mathematical model for the cell dynamics using the experimental data.

B. Autonomous control

To direct a cell to the desired position and orientation (x, y, θ) the RRT was implemented with feedback control. The cell was controlled in the same PDMS channel used in the

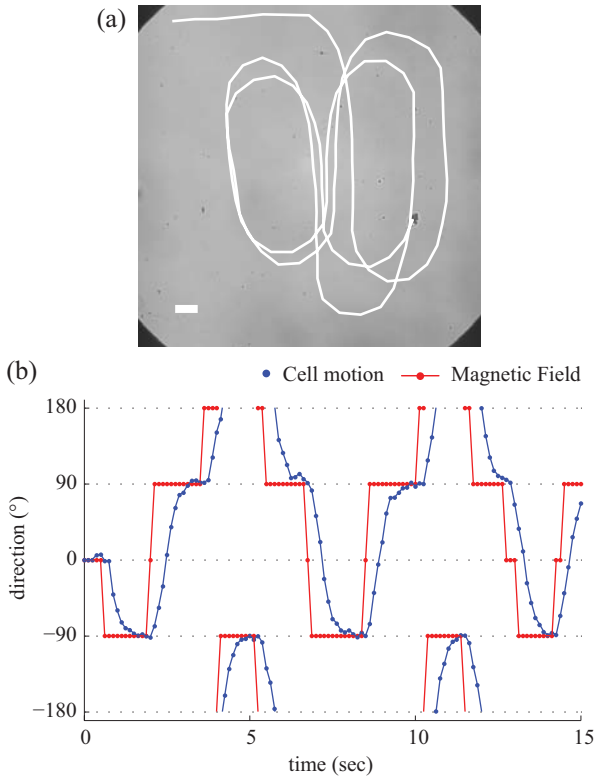

Fig. 5. Manual control of artificially magnetotactic *T. pyriformis*. (a) The traveled trajectory for the first 15 seconds. (b) The direction of the cell motion and magnetic field. The scale bar is 100 μm.

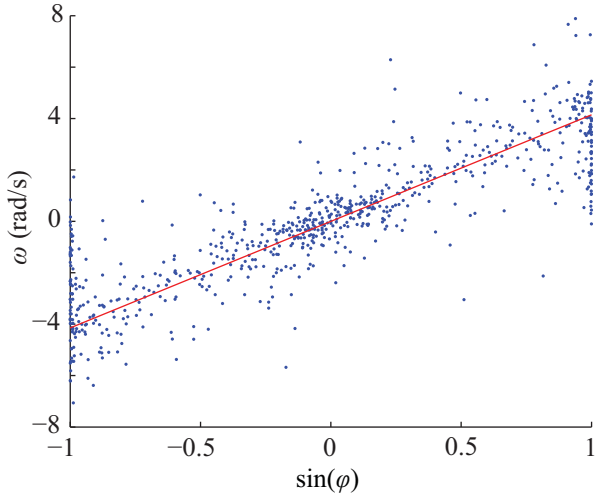

Fig. 6. The relation between the angular velocity and the angle ϕ, which is the angle between the cell motion and the magnetic fields. The slope of the regression line is 4.143 *rad/sec*.

experiment in Figure 5, and there is no physical obstacle and wall in the field of view. We generated 300 nodes randomly for the RRT in the field of view where is 2 *mm* by 2 *mm*. The total number of generated nodes was optimized from experiments to plan a path which passes through at most three nodes from the random start configuration to the final configuration.

For the rotational motion of the local path planner, the turning radius was set to 220 μm which is larger than the minimum turning radius of the normal cells. When the turning radius is set smaller than the minimum value, the cell cannot follow the radial trajectory. In addition, the minimum turning radius is hard to measure because each cell has a different value and depends on its instantaneous velocity. Thus, we set the turning radius to about two times larger than the average minimum turning radius, which is about 100 μm, so that it allows the cell to follow the trajectory of the rotational motion. Once the path is generated by the RRT, the intermediate targets are created in sequence along the path with a certain distance, which is set to 100 μm in this experiment.

The whole system was processed at 8 Hz for real-time control and the final configurations were located in the center with the different orientations. The current position and orientation is considered as the start configuration for path planning. Sometimes the cell does not move well or becomes temporary stuck to the bottom of the channel. In this case, the control of the cell is considered as a failure and the RRT creates a new feasible path from the current configuration.

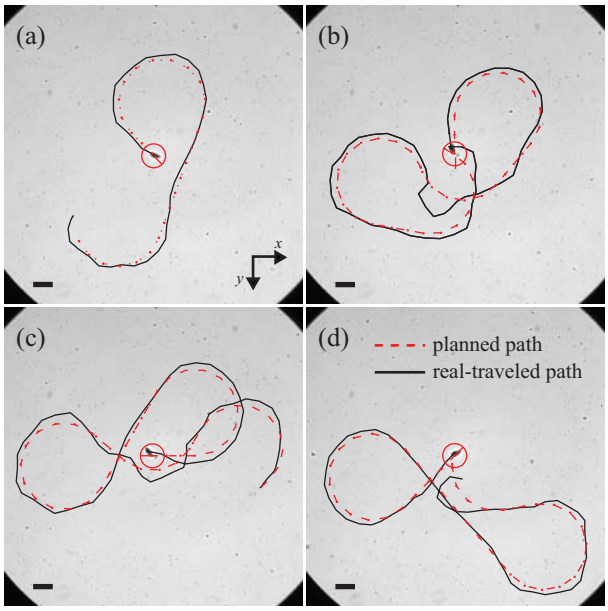

Fig. 7. Real-time feedback control with the RRT. (a)-(d) show the four different cases. The red dot lines are the planned paths by the RRT and the black solid lines are the traveled paths of magnetotactic *T. pyriformis*. The scale bar is 100 μm.

Figure 7 shows four different cases of feedback control with feasible path planning. The feasible path was planned

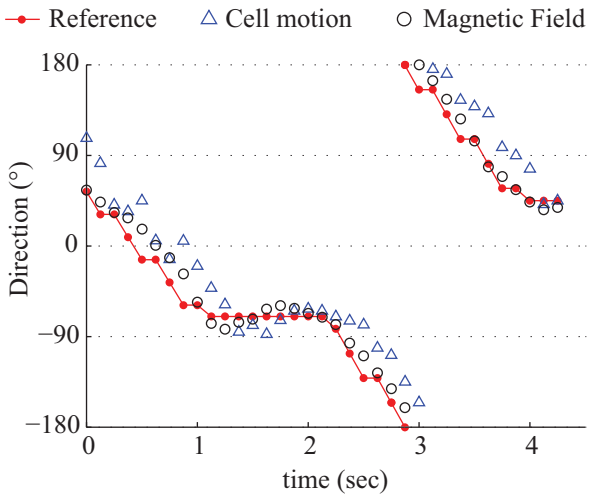

Fig. 8. Direction of motion of *T. pyriformis* (blue triangle), magnetic field direction (black circle), and reference between previous and current targets (red line) for real-time feedback control of *T. pyriformis*.

for the cell to approach the goal configuration with the desired orientation. The planned paths and real-traveled paths are represented by the red dot line and solid black line respectively. Figure 8 shows the direction of the cell motion (blue triangles) and the applied magnetic field (black circles) in the case of Figure 7 (a). The red reference line indicates the direction from the previous target point to the next target. The direction of the cell motion followed the reference line, which means that exerted torque from the angle between the direction of the cell motion and the direction of the magnetic field properly guided the cell to the target. Also, there are some transient responses after the reference line is changed, which is the same phenomena from the manual control experiment in Figure 5.

In summary, the relationship between the angular velocity and the torque provides a deeper understanding of the behavior of magnetotactic *T. pyriformis* under the magnetic field. In addition, the RRT, a path planning algorithm for nonlinear systems, is combined with feedback control to accomplish 3-dimensional (x, y, θ) control of *T. pyriformis*. This position and direction control of artificially magnetotactic *T. pyriformis* can be used for micro-scale engineering work.

V. CONCLUSIONS

In this paper, we introduce the artificially magnetotactic *T. pyriformis*, a eukaryotic cell, as a micro-bio-robot by internalizing magnetite into the cell body. In addition, real-time feedback control and the RRT for path planning was implemented for the biological system. The RRT was implemented as a path planner because it is simple and efficient at generating a feasible path for the nonlinear motion of *T. pyriformis*. Combining feedback control and the RRT allows the magnetotactic *T. pyriformis* to travel along the planned trajectory and finally reach the desired position with the desired orientation. Manual control provided understanding

of the cell's movement under the magnetic fields while real-time feedback control, with a feasible path planning scheme, showed the potential of employing *T. pyriformis* as micro-bio-robots to accomplish a variety of significant engineering and biotechnological tasks in microfluidic environments. We plan on enhancing the performance of this system by developing a more detailed mathematical model that describes the dynamics of the cell motion. To this end, we will use techniques from system identification [24] in conjunction with the experimental data that we have obtained. With a more detailed model, we expect to be able to predict the transient behavior of the system better, and have a better set of constraints to use for the RRT algorithm.

VI. ACKNOWLEDGMENTS

This work was funded by NSF CAREER Awards CMMI #0745019 and CBET #0828167

REFERENCES

[1] A. Ghosh and P. Fischer, "Controlled Propulsion of Artificial Magnetic Nanostructured Propellers," *Nano Letters*, vol. 9, pp. 2243-2245, 2009.

[2] L. Zhang, *et al*., "Artificial bacterial flagella: Fabrication and magnetic control," *Applied Physics Letters*, vol. 94, p. 064107, 2009.

[3] L. Zhang, *et al*., "Micromanipulation using artificial bacterial flagella," in *Intelligent Robots and Systems, 2009. IROS 2009. IEEE/RSJ International Conference on*, 2009, pp. 1401-1406.

[4] S. Floyd, *et al*., "An untethered magnetically actuated micro-robot capable of motion on arbitrary surfaces," in *Robotics and Automation, 2008. ICRA 2008. IEEE International Conference on*, 2008, pp. 419-424.

[5] M. Sakar, *et al*., "Single cell manipulation using ferromagnetic composite microtransporters," *Applied Physics Letters*, vol. 96, p. 043705, 2010.

[6] S. Martel, *et al*., "Towards swarms of communication-enabled and intelligent sensotaxis-based bacterial microrobots capable of collective tasks in an aqueous medium," *in Robotics and Automation, 2009. ICRA '09. IEEE International Conference on*, 2009, pp. 2617-2622.

[7] S. Martel, *et al*., "Flagellated Magnetotactic Bacteria as Controlled MRI-trackable Propulsion and Steering Systems for Medical Nanorobots Operating in the Human Microvasculature," *The International Journal of Robotics Research*, vol. 28, pp. 571-582, April 2009 2009.

[8] S. Martel, *et al*., "Controlled manipulation and actuation of micro-objects with magnetotactic bacteria," *Applied Physics Letters*, vol. 89, p. 233904, 2006.

[9] B. Behkam and M. Sitti, "Effect of quantity and configuration of attached bacteria on bacterial propulsion of microbeads," *Applied Physics Letters*, vol. 93, p. 223901, 2008.

[10] M. S. Sakar, *et al*., "Modeling, control and experimental characterization of microbiorobots," *International Journal of Robotics Research*, vol. Accepted, 2010.

[11] E. Steager, *et al*., "Control of microfabricated structures powered by flagellated bacteria using phototaxis," *Applied Physics Letters*, vol. 90, pp. 263901-3, 2007.

[12] D. H. Kim, *et al*., "Galvanotactic and phototactic control of *Tetrahymena pyriformis* as a microfluidic workhorse," *Applied Physics Letters*, vol. 94, p.163901, 2009.

[13] A. Itoh, *et al*., "Motion Control of Euglena Group by Weak Laser Scanning System and Object Manipulation Using Euglena Group," in *Advanced Intelligent Mechatronics. Proceedings, 2005 IEEE/ASME International Conference on*, 2005, pp. 43-47.

[14] A. Itoh, "Motion control of protozoa for bio-MEMS," *Mechatronics, IEEE/ASME Transactions on*, vol. 5, pp. 181-188, 2000.

[15] N. Ogawa, *et al*., "A physical model for galvanotaxis of Paramecium cell," *Journal of Theoretical Biology*, vol. 242, pp. 314-328, 2006.

[16] L. Köhidai and G. Csaba, "Effects of the mammalian vasoconstrictor peptide, endothelin-1, on *Tetrahymena pyriformis* GL, and the immunocytological detection of endogenous endothelin-like activity," *Comparative Biochemistry and Physiology Part C: Pharmacology, Toxicology and Endocrinology*, vol. 111, pp. 311-316, 1995.

[17] D. H. Kim, *et al*., "Artificial magnetotactic motion control of *Tetrahymena pyriformis* using ferromagnetic nanoparticles: A tool for fabrication of microbiorobots," *Applied Physics Letters*, vol. 97, p.173702, 2010.

[18] J. L. Rifkin and R. Ballentine, "Magnetic Fettering of the Ciliated Protozoon *Tetrahymena pyriformis*," *Transactions of the American Microscopical Society*, vol. 95, pp. 189-197, 1976.

[19] J. William H. Hayt and J. A. Buck, *Engineering electromagnetics*, 7th edition ed. New York: McGraw-Hill, 2006.

[20] D. H. Kim, et al., "Practical motion planning for car-parking control in narrow environment," *Control Theory & Applications*, vol. 4, pp. 129-139, Jan. 2010 2010.

[21] J. Reeds and L. Shepp, "Optimal paths for a car that goes both forwards and backwards," *Pacific Journal of Mathematics*, vol. 145, pp. 367-393, 1990.

[22] S. LaValle and J. Kuffner Jr, "Randomized kinodynamic planning," *The International Journal of Robotics Research*, vol. 20, p. 378, 2001.

[23] S. M. LaValle, *Planning Algorithms*: Cambridge University Press, 2006.

[24] L. Ljung and E. Ljung, *System identification: theory for the user*: Prentice-Hall Englewood Cliffs, NJ, 1987.